2016

Analytic ab initio-based molecular interaction potential for the $BrO{\cdot}H_2O$ complex

Ross D. Hoehn
Purdue University

Sachin D. Yeole
Purdue University

Sabre Kais
Purdue University

Joseph S. Francisco
University of Nebraska-Lincoln, frjoseph@sas.upenn.edu

Analytic *ab initio*-based molecular interaction potential for the $BrO{\cdot}H_2O$ complex

Ross D. Hoehn,[1,2] Sachin D. Yeole,[1] Sabre Kais,[1,2] and Joseph S. Francisco[1,3,a)]
[1]*Department of Chemistry, Purdue University, West Lafayette, Indiana 47907, USA*
[2]*Qatar Environment and Energy Research Institute, HBKU, Doha, Qatar*
[3]*Departments of Chemistry, University of Nebraska, Lincoln, Nebraska 68588, USA*

(Received 15 February 2016; accepted 9 May 2016; published online 27 May 2016)

Radical halogen oxide species play important roles within atmospheric processes, specifically those responsible for the removal of O_3. To facilitate future investigations on this family of compounds, RCCSD(T)/aug-cc-pVQZ-level electronic structure calculations were employed to generate individual-molecule optimized geometries, as well as to determine the global minimum energy structure for the $BrO{\cdot}H_2O$ complex. This information facilitated the generation of several one-dimensional potential energy surface (PES) scans for the $BrO{\cdot}H_2O$ complex. Scans were performed for both the ground state and the first excited state; this inclusion is due to a low-lying first electronic excited-state energy. These rigid-geometry PES scans were used both to generate a novel analytic interaction potential by modifying the existing Thole-type model used for water and to the fitted potential function. This interaction potential features anisotropic atomic polarizabilities facilitating appropriate modeling of the physics regarding the unpaired electron residing within the p-orbitals of the oxygen atom of the bromine oxide radical. The intention of this work is to facilitate future molecular dynamics simulations involving the interaction between the BrO radical and water clusters as a first step in devising possible novel chemistries taking place at the water interface of clouds within the atmosphere. *Published by AIP Publishing.* [http://dx.doi.org/10.1063/1.4950956]

I. INTRODUCTION

Enhanced concentration of halogens within the atmosphere has been indicted as a contributing factor to the depletion of the ozone layer, both in the stratosphere and in the marine boundary-layer.[1–10] Depletion of ozone within these regions is due in large part to the important roles which halogen oxide species, such as ClO and BrO, play in the destructive processes. Careful examination of the chemistries involved with such species while they interact with water clusters should be performed and replicated for similar radicals.[11,12] This interaction has been shown through *ab initio* calculations to permit the generation of non-planar water-$ClO^{\cdot}$ complexes which may act as chaperone complexes in the formation of ClOOCl, and whose photodecomposition product is the $Cl^{\cdot}$ vital in ozone depletion.[13,14] Bromine containing radical species have been found to be more effective than the chlorine analogues in the processes destroying ozone. The catalytic mechanism underlying the ozone depletion involving bromine is well-established;[4–7] this catalytic cycle is described in Equation (1)

$$\begin{aligned} Br^{\cdot} + O_3 &\longrightarrow BrO^{\cdot} + O_2, \\ BrO^{\cdot} + h\nu &\longrightarrow Br^{\cdot} + O^{\cdot}, \\ O^{\cdot} + O_3 &\longrightarrow 2O_2. \end{aligned} \tag{1}$$

This cycle, involving bromine and the bromine monoxide radical, plays a crucial role in ozone depletion within the marine boundary layer. The major sources of both Br and $BrO^{\cdot}$ within the marine boundary layer include: sea salt aerosols, (poly)halogenated compounds, and marine algae.[15–19] Deep convection processes loft these bromine species and — after decomposition — atomic bromine is generated within the global troposphere. Additionally, a significant source of stratospheric bromine is agricultural-derived halons.[20,21] Hydrogen-bonded complexes composed of free radicals and water play important roles in atmospheric reactions, especially on droplet surfaces where steric confinement promotes the generation of specific chemical products.[5–14,22–32] The interactions between both the OH radical and the ClO radical each individually with water molecules have been investigated in detail both experimentally and theoretically.[11–14,23–31] However, bromine and its monoxide radical have been the subject of very few of such investigations.[33,34]

Gálvez *et al.*[33] have reported the equilibrium structures, the energetics, and the properties of the BrO-hydrates using density functional theory coupled with second order Moller-Plesset perturbation theory. In an additional study, Gálvez *et al.*[34] employ stationary state methods to characterize the interactions involved in the formation of halogen oxides and water molecule complexes by electron density analysis.[34] These previous works concentrate on stationary point calculations, yet it is essential to generate an effective map of the PES of this complex both to model chemical processes and to facilitate dynamic molecular simulations. To date, there exist few studies that have systematically investigated the potential energy surface (PES) of the $BrO{\cdot}H_2O$ complex; such studies would enable future investigations

a)Author to whom correspondence should be addressed. Electronic mail: jfrancisco3@unl.edu

concerning the governing interactions of the BrO radical — both in the atmosphere and in liquids — and their most likely reaction products. The present paper should act as a first step in modeling the physics and the dynamic interactions between this vital radical species, as well as assist in the determination of its atmospheric chemistries.

Within the present work, we report several 1-dimensional potential energy surface scans of the $BrO{\cdot}H_2O$ complex, and from these scans we generate the parameters for an analytic interaction potential function; this is done in effort to facilitate future molecular dynamics studies of this important atmospheric aerosol radical at the surface of water clusters. As noted in earlier studies concerned with both the OH and the ClO radicals,[11,12] the excited state energies of these systems lay very close to the ground state energies. The proximity of the ground and excited states is suggestive of the excited state playing an important role in determining the energy dynamics of these complexes under both atmospheric conditions and solar irradiation. Furthermore, the open shell nature of the $^2\Pi$ BrO radical interacts with the closed shell water in such a way to cause energy splitting of its low-laying electronic states. These states differ in which p-orbital is singly occupied, either an in-plane or an out-of-plane state is possible, each state presenting a unique anisotropic polarizability and different reactivity. Additionally, the interactions between open shell atoms and specific closed shell species have been shown to alter the nature of solvation and the associated solvation structures for the open shell species. Considering this, several 1-dimensional scans of the PES were generated for both the ground and the excited states. These scans were generated by restricted coupled cluster theory [RCCSD(T)], describing single and double excitations, while employing a perturbation theory estimation for the triple excitations.[35–38] Consistent with earlier approaches used for both the $OH{\cdot}H_2O$ and the $ClO{\cdot}H_2O$ complexes,[11,12] the PES scans are fitted to an analytical potential. The selected potential is a modification of the Thole-type model (TTM); the mTTM was originally developed for water-water interaction[39–42] and is available within the AMBER molecular dynamics suite. This model modifies the Thole-type model through all atom, anisotropic polarizabilities upon a rigid molecule framework.

II. METHODOLOGY

A. Computational details

The one-dimensional PES scans of the $BrO{\cdot}H_2O$ complex were generated at the RCCSD(T) level of theory and by using the Dunning augmented-correlated consistent valence polarized quadruple zeta basis set (aug-cc-pVQZ).[43,44] Sequential analysis of basis sets was foregone within this work for similar reasons as previous works.[11,12] Large-scale *ab initio* calculations of the binding energy of the water dimer have been performed and it was found that for the OH radical system the aug-CC-pVTZ basis was in good agreement with the basis set limit for the interaction potential.[26] We have opted to use the aug-cc-pVQZ basis to assure a good description of the expanded orbitals and greater polarizability of the Br atom. Furthermore, related basis sets have been shown to be more than adequate choices for obtaining the energy from all electron RCCSD(T) calculations.[35,45–47] BSSE calculations were performed; the BSSE associated with the global minima was found to be 0.13 kcal/mol, compared to the total uncorrected IE of 4.38 kcal/mol. The counterpoise corrections performed for radial Scan 1 revealed a maximum error found to be 0.55 kcal/mol at the most divergent point of the binding energy. Scan 4 was also examined and the maximum error was found to be 0.234 kcal/mol. The inclusion of BSSE corrections did not alter the nature of the interaction energy scans, for this reason BSSE corrections were forgone in this work. Additionally, the bromine atom — and molecules formed from it — has displayed some pronounced relativistic effects.[48–52] We are concerned herein with interaction energies between the BrO radical and a water molecule; as the main contributions to relativistic effects on valence electrons, such as Breit contributions, are smaller (on the order of α^2, where α is the fine structure constant) than the accuracy of most quantum calculation methods, so they may be disconsidered. Additionally, non-covalent corrections such as Gaunt corrections can have significant effects on the lowest electronic state of molecules,[51] yet its properties are mainly determined by the innermost electrons and will have greatest effect on the total energy and not the interaction energy of the dimer. Within this work we employ a non-relativistic Hamiltonian, with no spin-orbit coupling (SOC). It is known that the Br_2 molecule requires computation to be performed with consideration given to both electron correlation and relativistic effects.[48] While bound to an oxygen atom, as in the OBr radical, the SOC contributions should be less than the Br_2 system, but the importance of electron correlation will remain. Electron correlations where treated through restricted coupled cluster scheme, full configuration interaction calculation would be too costly to be performed on this system.

Inspired by previous works discussing the $OH{\cdot}H_2O$ and $ClO{\cdot}H_2O$ dimers,[11,12] all the PES scans for our $BrO{\cdot}H_2O$ dimer were generated by calculating approximately 30-40 calculated stationary points for the dimer complex while scanning a single intermolecular degree-of-freedom; this procedure generates a 1-dimensional slice of the full PES along a particular degree-of-freedom. This procedure was repeated, thereby generating several characteristic slices of the PES for the fitting procedure to a 3-dimensional analytic function. The binding energy (BE) of a stationary point along the PES is calculated as the difference between the energy of the corresponding geometric configuration of the $BrO{\cdot}H_2O$ complex and the sum of individual energies of the optimized constituent molecules at the RCCSD(T)/aug-cc-pVQZ level of theory. These *ab initio* calculations were carried out using the MOLPRO quantum chemistry suite.[53,54]

B. Analytical model

Herein, we have selected the rigid TTM2-R model to describe the water potential; furthermore, we have generated a modified Thole-type model (U^{mTTM}) to describe the dimer-interactions between a BrO radical and a water molecule. This model employs a smeared-charge description, whereby

the smeared-charges allow for an expansion of the Coulombic interaction term to include charge-dipole and dipole-dipole terms, as well as the standard charge-charge interaction. The total interaction potential for the $BrO{\cdot}H_2O$ complex is then given as:

$$U^{mTTM} = U^{pair} + U^{elec} + U^{ind}. \tag{2}$$

The terms within Equation (2) are: U^{ind} describes the induction energy of the system; U^{elec} is an electrostatic interaction term describing the Coulombic, as well as the charge-dipole and dipole-dipole interactions for the smeared charges; and U^{pair} is a pairwise Lennard-Jones attraction-repulsion term over each interaction site. The mTTM model adopts a rigid 3-site model for water, these being the hydrogen sites and an "M" site located along oxygen's bisector between the two hydrogen. This "M" site houses the charge, and thus the interactions, associated with the oxygen atom. The model is adapted to the halide-oxygen radical system by using a two-site description: the halide and an "M" site for the oxygen

We have used the original form of the U^{elec} term as proposed for the TTM2-R model of Burnham and Xantheas[40] The forms of the remaining two terms must be slightly altered to explicitly describe the $BrO{\cdot}H_2O$ system; therefore, all alterations described herein are only for application to the BrO radical system. For a more complete discussion of each term, we direct the reader to previous works.[39,40,42] The complete form of the electrostatic term — used in the aforementioned references — is given here

$$U^{elec} = \sum_{i<j} (Q_i Q_j \phi(r_{ij}, a^{CC}) + (\mathbf{D}_i Q_j - Q_j \mathbf{D}_i) \cdot \nabla_r \phi(r_{ij}, a^{CD}) - \mathbf{D}_j \mathbf{D}_j \cdot \nabla_r \nabla_r \phi(r_{ij}, a^{DD})). \tag{3}$$

The leading double sum is over all charge-dipole sites and the index constraint prevents the double counting of interactions; within Equation (3), Q_i and $\mathbf{D}_i$ are the charge and dipoles on the ith site and $\phi(r, a)$ is a screened Coulomb interaction. The form of $\phi(r, a)$ is

$$\phi(r_{ij}, a) = \frac{1}{r_{ij}}(1 - exp[-a(r_{ij}/A_{ij})^3] + a^{1/3}(r_{ij}/A_{ij})\Gamma(2/3, a(r_{ij}, /A_{ij})^3)), \tag{4}$$

where a is a width parameter, r_{ij} is the linear distance between sites i and j, $\Gamma(c, x)$ is the incomplete gamma function over variable x with width c, and $A_{ij} = (\alpha_i \alpha_j)^{1/6}$ where α_i is the average of the diagonal components of the ith atoms polarizability tensor.[40] The width parameter a is allowed to vary for the specific site-site interaction type as within Burnham:[42] charge-charge, $a^{CC} = 0.2$; charge-dipole, $a^{CD} = 0.2$; and dipole-dipole, $a^{DD} = 0.3$.

The Lennard-Jones pairwise interaction term, U^{pair}, for the $BrO{\cdot}H_2O$ system can be written as

$$U^{pair} = \sum_k \left[4\epsilon_{OO} \left[\left(\frac{\sigma_{OO}}{r_{OO,k}}\right)^{12} - \left(\frac{\sigma_{OO}}{r_{OO,k}}\right)^{6} \right] + 4\epsilon_{OBr} \left[\left(\frac{\sigma_{OBr}}{r_{OBr,k}}\right)^{n_1} - \left(\frac{\sigma_{OBr}}{r_{OBr,k}}\right)^{m_1} \right] + 4\epsilon_{HO} \sum_{i=1,2} \left[\left(\frac{\sigma_{HO}}{r_{HO,k}}\right)^{n_2} - \left(\frac{\sigma_{HO}}{r_{HO,k}}\right)^{m_2} \right] + 4\,\epsilon_{HBr} \sum_{i=1,2} \left[\left(\frac{\sigma_{HBr}}{r_{HBr,k}}\right)^{n_3} - \left(\frac{\sigma_{HBr}}{r_{HBr,k}}\right)^{m_3} \right] \right]. \tag{5}$$

Within the above, the sum over k counts the number of water molecules within the system; k is taken to be 1 for the present parameterization. The ϵ_{XY} terms retain their standard significance as the Lennard-Jones two-term interaction energy between atoms X and Y; σ_{XY} is the distance parameter for the interaction between atoms X and Y, representing the point where the potential crosses zero on the energy axis; and r_{XY} is the radial distance between atoms X and Y. Finally, the induction term is given by

$$U^{ind} = \sum_{i=1} \left(\frac{\mathbf{D}^2_{\mathbf{x,i}}}{2\alpha_{xx,i}} + \frac{\mathbf{D}^2_{\mathbf{y,i}}}{2\alpha_{yy,i}} + \frac{\mathbf{D}^2_{\mathbf{z,i}}}{2\alpha_{zz,i}} \right); \tag{6}$$

where $\mathbf{D_{x,i}}$ is the xth component of the dipole associated with the ith atom and $\alpha_{xx,i}$ is the diagonal component in the xth direction of the ith atom's polarizability tensor. This term captures the energy expenditure associated with the anisotropic polarization of each atom with the system.

In fitting the analytical potential to the *ab initio* values and geometries, the optimization expression, f, as a function of the collection of parameter values, p_i, was employed

$$f(p_1, p_2, \ldots, p_{22}) = \sum_{i}^{N_{scans}} \sum_{j}^{N_{points,i}} \left[U^{ab}(\mathbf{g}_{i,j}) - U^{mTTM}(\mathbf{g}_{i,j}, p_1, p_2, \ldots, p_{22}) \right]^2 \cdot w_{i,j}. \tag{7}$$

Within the above N_{scans} and $N_{points,i}$ are the number of scans and the number of energy points within the ith scan. U^{ab} is the value of the *ab initio* energy associated with the molecular configuration and geometry $\mathbf{g_{i,j}}$. U^{mTTM} is the modified-Thole-type potential whose physical and Lennard-Jones parameters are being fitted at each fixed $\mathbf{g_{i,j}}$. $w_{i,j}$ are weighting factors for each point per scan; for radial(angular) scans the weighting factor was set to 1.0(0.8) for all points but the minimum,

which was assigned a value of 20(10). This weighted sum of roughly 196 functional terms — entirely governed by the local geometry and 22 parameters — was then minimized.

III. RESULTS AND DISCUSSION

A. Potential energy scans

In generating PES scans of the BrO·H_2O complex, the RCCSD(T)/aug-cc-pVQZ optimized geometries of both the BrO radical and the water molecule were maintained while varying the intermolecular geometry between the two molecules. This methodology has been adopted to build the rigid, analytic interaction PES's for the system for use in future molecular dynamics simulations. In the previous studies, it has been observed that the changes in the internal coordinates of the individual molecules within a complex are small as compared to free molecules; therefore, geometric relaxation of the two monomers was not considered herein.[11,12] In the RCCSD(T) optimized geometry for the water molecule, the values of the O–H bond length, r_{OH}, and the angle $\angle_{HOH}$, θ_w, are 0.959 Å and 104.355°, respectively. The BrO bond length, r_{BrO}, in RCCSD(T) optimized structure is found to be 1.724 Å. The internal coordinate system used for generating the PES scans is depicted in Figure 1. Here, the water molecule is set in the xy-plane such that the O atom (O_1) coincides with the origin and a OH bond coincides with the positive direction along the x-axis. The BrO molecule is also oriented along the positive x-axis; the distance between O_1 and the oxygen atom in BrO (O_2) defining $R_{O..O}$. The coordinates of the water molecule are fixed and its internal coordinates are entirely defined by its optimized geometric parameters, r_{OH} and θ_w, whereas the intermolecular coordinates of the BrO molecule are obtained through new spherical coordinates θ, ϕ, θ', and ϕ', as well as the inter-oxygen distance, $R_{O..O}$ (see Figure 1); thereby, the geometry of the entire complex is completely defined by the fixed internal coordinates and five intermolecular, spatial degrees-of-freedom. The one-dimensional PES scans are then generated by varying a single coordinate of the intermolecular geometry and fixing the remaining four degrees-of-freedom. The values assigned to each intermolecular degree-of-freedom used to generate the seven in Table I, where the final scan is to be used as a test

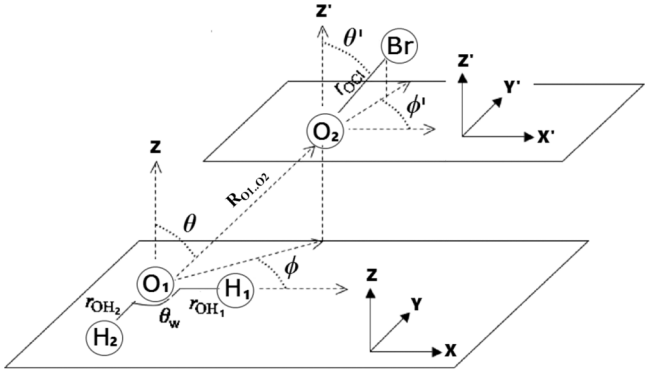

FIG. 1. Graphical representation defining the intermolecular coordinate system for the BrO·H_2O complex.

TABLE I. Geometric variables chosen for the potential energy surface scans of the BrO·H_2O complex. Distances are in angstroms and angles are in degrees.

Scan no.	$R_{O..O}$ (Å)	θ (deg)	ϕ (deg)	θ' (deg)	ϕ' (deg)
1	Variable	90	0	90	70
2	Variable	87	128	93	−52
3	Variable	90	−52	90	−52
4	3.125	90	0	90	Variable
5	4.560	87	128	Variables	−52
6	3.000	Variable	−52	$=\theta$	−52
Test scan	3.125	90	Variable	90	$=\phi$

of the fitted parameters. In order to specify the ground and excited state by symmetry number, each series of calculations for a scan is initialized with at least C_S symmetry. The corresponding interaction potential scans obtained through RCCSD(T)/aug-cc-pvQZ calculations and employed in the fitting procedure are displayed in Figures 2–11, each figure has an inlay showing the relative orientations of the two monomers and specifying the degree-of-freedom to be varied. The zero point of the interaction potential is defined to be the energies of the two molecules at the limit of infinite separation and the binding energy (BE) is defined as the difference between the minimum value of the interaction energy and the zero point energy.

In the first PES scan, the radial coordinate $R_{O..O}$ is varied, as seen in Table I; the BE of this scan is shown in Figure 2. It is clear that the vital interactions present in this scan is the balance between the attractive O_2–H interaction and the on-set of the O_1–O_2 repulsion. The angle $\angle_{Br-O_2-O_1}$ is held at 70°, which is nearer the minimum value obtained from the scan over this angle, see Scan 4. Similar to the OH·H_2O and the ClO·H_2O potentials, the ground and excited states have A″ and A′ symmetries, respectively. The minimum energy value for $R_{O..O}$ occurs at 3.10 Å (2.57 kcal/mol) and 3.10 Å (2.03 kcal/mol) for the ground and excited states,

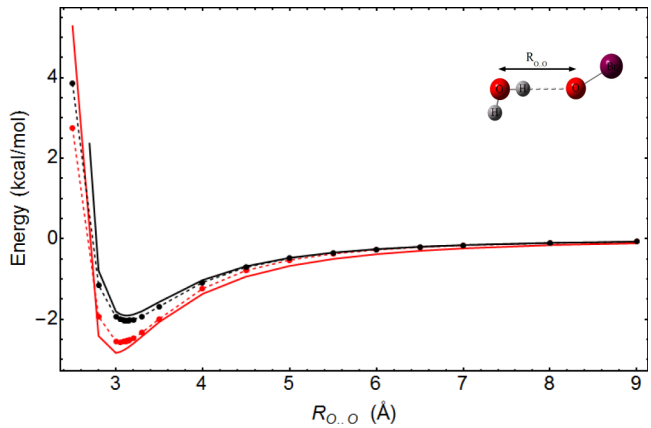

FIG. 2. Potential energy as a function of the distance $R_{O_1..O_2}$ for the ground and first excited states of the BrO radical interacting with water calculated at RCCSD(T)/aug-cc-pVQZ. Red lines denote ground state and black curve denotes the excited state. Dashed curves are from RCCSD(T)/aug-cc-pVQZ with dots at the exact location of each data point, while solid curves are for mTTM potential energies. Values of R_{OO}, θ, ϕ, θ', and ϕ' parameters taken from Table I - Scan 1. See text for details.

respectively. The $R_{O..O}$ distances at the minimum interaction energy are comparable to that of the $OH{\cdot}H_2O$ (3.00 Å and 3.20 Å) and the $ClO{\cdot}H_2O$ (3.05 Å and 3.20 Å) systems. The BE energy for the ground state is less than that of $ClO{\cdot}H_2O$ by 0.54 kcal/mol while the excited state energy is higher by 0.5 kcal/mol. This results in a much lower energy splitting (0.54 kcal/mol) when compared to the $OH{\cdot}H_2O$ (2.1 kcal/mol) or the $ClO{\cdot}H_2O$ (1.53 kcal/mol) system. This is likely due to the large size of the Br atom and the large variation in polarization effects shown by the Br atom while within the BrO radical compared to the Cl atom within the ClO radical.[34] The ground state minimum geometry shows good agreement with the optimized local minimum structure; this optimized local structure, near the minimum, shows a slight alteration of angle laying along Scan 4, at a 78° angle rather than 70°. The optimized structure has a BE of 2.80 kcal/mol and an $R_{O..O}$ distance of 3.05 Å, compared to a BE of 2.57 kcal/mol and an $R_{O..O}$ of 3.10 Å in ground state PES.

The second scan is also performed over $R_{O..O}$, where the dominant contributions are from the Br atom forming a weak bond with the O_1 atom of the water molecule (see Figure 3). In this configuration, the $\angle_{O_1-Br-O_2}$ angle is kept at 180° with the BrO radical above the molecular plane of the water molecule at an angle of 3°. The minima occur at an $R_{O..O}$ value of 4.56 Å and of 4.61 Å for the ground and excited state, respectively. The corresponding BEs are 4.36 kcal/mol and 3.96 kcal/mol, respectively. Here these BEs and the corresponding $R_{O..O}$ distances of both the ground and the excited states are larger than the analogous configuration from the $ClO{\cdot}H_2O$ system. However, the energy splitting between the two states (0.4 kcal/mol) is comparable with the analogous configuration from both the $OH{\cdot}H_2O$ (0.32 kcal/mol) and the $ClO{\cdot}H_2O$ (0.3 kcal/mol) complexes. Similar to observations from the $ClO{\cdot}H_2O$ work, the geometry at the minimum of this scan is close to the optimized global minimum at the same level of theory, which has a stronger BE by 0.2 kcal/mol. The BrO_1 distance is 2.836 Å at the minimum of Scan 2; this value is in excellent agreement with the distance (2.834 Å) associated with the global minimum geometry. This suggests that the PES is capable of reproducing the global minimum.

In the third scan, the BrO radical is placed on the vector bisecting the $\angle_{H-O_1-H}$ angle of the water molecule and the $R_{O..O}$ parameter is varied; this scan captures the interactions between O_1 of water with O_2 of the BrO radical. The binding energies for the minimum of ground and excited states are 1.98 kcal/mol (at 3.0 Å) and 1.49 kcal/mol (at 3.16 Å), respectively. The binding energies and $R_{O..O}$ distances at the minimum for the two states are similar to those of both the $OH{\cdot}H_2O$ and the $ClO{\cdot}H_2O$ complexes for analogous configurations. The energy splitting between the ground and excited state BE's (i.e., 0.49 kcal/mol) is nearly identical to those of the $OH{\cdot}H_2O$ and the $ClO{\cdot}H_2O$ systems (0.49 kcal/mol and 0.48 kcal/mol, respectively). This identical behavior between systems is attributable to the fact that the BE energy of this series of scans is largely reflective of the interaction between O_1 and O_2 and the O_2–H interactions; the Br atom (Cl and H in previous studies) provides a diminutive contribution on the BE for this scan. The ground state minimum ($R_{O..O}$ = 3.0 Å) shows fair agreement with the optimized local minimum structure ($R_{O..O}$ = 3.13 Å) with a BE of 1.53 kcal/mol, as can be noted in Figure 4. This ground state minimum structure will be revisited in forthcoming Scan 6 and the test scan, where the test scan (to be discussed in Sec. III C suggests) that this is a saddle point along the angular ϕ degree-of-freedom and Scan 6 shows the minimum of Scan 3 to be an energy minimum along its rotation.

Scan 4 is an angular scan formulated from the configuration at the minimum of Scan 1 by wagging the Br atom within the xy-plane; thus varying the 70° off axis angle of Br. In this planar configuration, the angular degree-of-freedom ϕ' is varied from 90° to 90°, pin wheeling the Br atom around the O_2 of the BrO radical (see Figure 5). In the ground state, two minima are found at $\phi' = \pm 70°$ with binding energies 3.25 and 2.84 kcal/mol, respectively. These minima are characterized within the Lennard-Jones terms; the pin wheeled Bromine first interacts with the oxygen in an attractive manner and then becoming close enough for

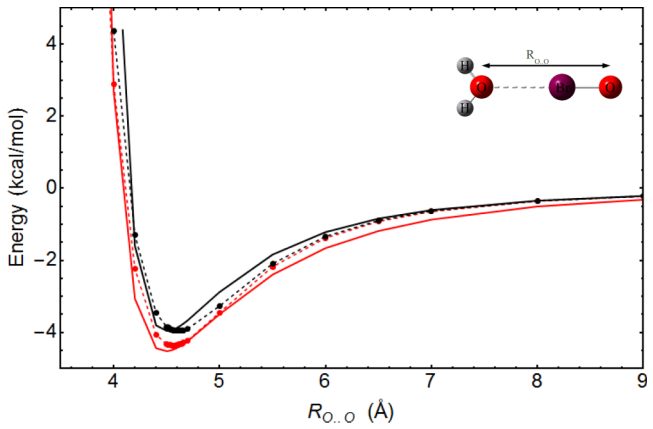

FIG. 3. Values of R_{OO}, θ, ϕ, θ', and ϕ' parameters taken from Table I - Scan 2. Red lines denote ground state and black curve denotes the excited state. Dashed curves are from RCCSD(T)/aug-cc-pVQZ with dots at the exact location of each data point, while solid curves are for mTTM potential energies.

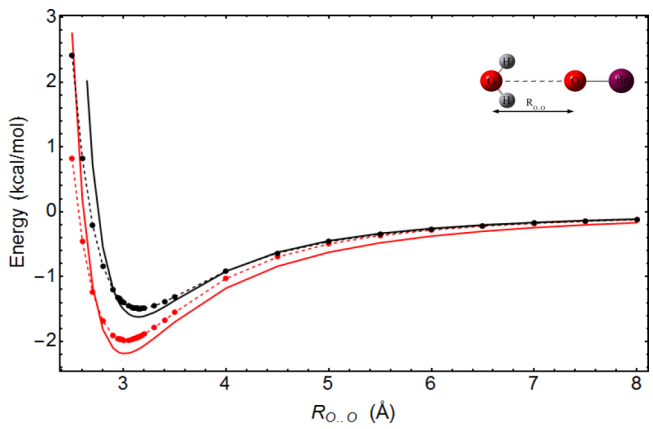

FIG. 4. Values of R_{OO}, θ, ϕ, θ', and ϕ' parameters taken from Table I - Scan 3. Red lines denote ground state and black curve denotes the excited state. Dashed curves are from RCCSD(T)/aug-cc-pVQZ with dots at the exact location of each data point, while solid curves are for mTTM potential energies.

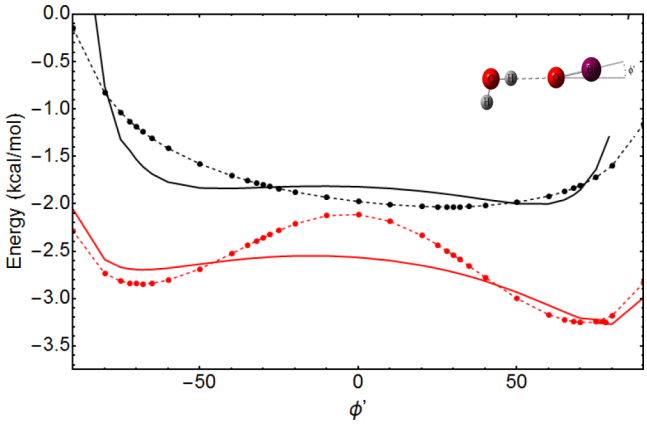

FIG. 5. Values of R_{OO}, θ, ϕ, θ', and ϕ' parameters taken from Table I - Scan 4. Red lines denote ground state and black curve denotes the excited state. Dashed curves are from RCCSD(T)/aug-cc-pVQZ with dots at the exact location of each data point, while solid curves are for mTTM potential energies.

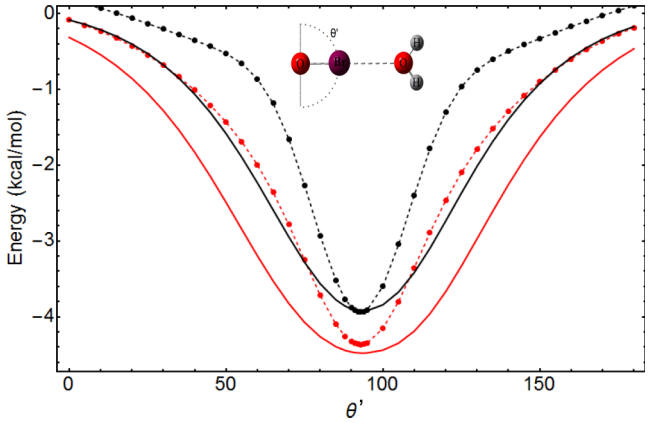

FIG. 6. Values of R_{OO}, θ, ϕ, θ', and ϕ' parameters taken from Table I - Scan 5. Red lines denote ground state and black curve denotes the excited state. Dashed curves are from RCCSD(T)/aug-cc-pVQZ with dots at the exact location of each data point, while solid curves are for mTTM potential energies.

contributing repulsive forces with the hydrogen due to the relative size of the crossing points, σ's. The relative stability of the two minima in the ground state is clearly due to the presence of the second hydrogen, making the pin wheeling motion asymmetric. This asymmetry is further present in the A″ state, yet due to the decreased polarizability in the y-direction the minima are not pronounced. In the excited state PES, a single minimum was found at $\phi' = 30°$ (2.03 kcal/mol). This behavior is likely due to a larger anisotropic character in the polarizability of Br in the ground state causing larger stabilization than the largely similar directional polarizabilities in the excited state. The two energy states have very proximate energies at $\phi' = 0°$ which is a maximum for the ground state; this proximity may allow for nonadiabatic transitions between the ground and excited states and therefore engenders the likely state mixing justifying the consideration of both the ground and excited state PESs. All the BEs of minimum and maximum in ground state are higher than those of the ClO·H_2O potential in analogous configurations. Similar to the OH·H_2O and ClO·H_2O systems, the BEs of the ground and excited states are very close and the splitting increases as ϕ approaches ±90°; this is due to the pinwheeling Br interaction with the hydrogen of the water.

Scan 5 is shown in Figure 6. This PES slice fixes all intermolecular degrees-of-freedom except the angular variable θ', with $R_{O..O}$ fixed at 4.4 Å; within this scan, at $\theta' = 93°$ we obtain a configuration which is close to minimum of Scan 2. Here the Br atom is again pin wheeled by varying θ' so that it allows a configuration where the O–Br bond is perpendicular to the water's molecule plane. This scan facilitates good characterization of the Br–O_2 interaction as it holds all other interaction parameters roughly constant. It is obvious from the *ab initio* values that the ϵ_{OBr} will be fairly large. The symmetry of this plot, compared to the previous scan, is due in large part to the orientation of the water, such that the frozen value of $\theta' = 90°$ enforces C_{2v} symmetry. Both ground and excited states have their minima at $\theta' = 93°$ with binding energies of 4.36 and of 3.94 kcal/mol, respectively. The energy splitting between the ground and excited state at the minimum is 0.42 kcal/mol, almost identical to that in the ClO·H_2O potential. The larger energy gap is observed in the ranges where ϕ is between 40°-70° and 120°-150°. The minimum of this scan is the same as the minimum of Scan 2 with identical BEs, and hence a similar structure to the global minimum.

In Scan 6, both ϕ and ϕ' are set to −52° and angular coordinate θ is varied from an initial value placing the BrO radical along the bisector of $\angle_{HOH}$ angle in water (see Figure 7). The BrO radical is then rotated around O_1 maintaining collinearity of O_1–O_2–Br with an equiangular relationship to each hydrogen. This scan is clearly most characteristic of varying the interaction distance between the attractive O_2–H and the repulsive O_1–O_2 forces. The distance $R_{O..O}$ is set to 3.0 Å, corresponding to the minimum of Scan 3. Both the ground and excited states have their minimum at $\theta = 90°$ with the BEs 1.93 kcal/mol and 1.49 kcal/mol, respectively. The energy splitting is maximum at $\theta = 90°$ and decreases toward $\theta = 0°$. The energy splitting at the minimum is 0.44 kcal/mol, slightly lower than that of the ClO·H_2O potential (0.55 kcal/mol). The minimum of Scan 6 is close to the minimum in Scan 3, which is a maximum in the test scan.

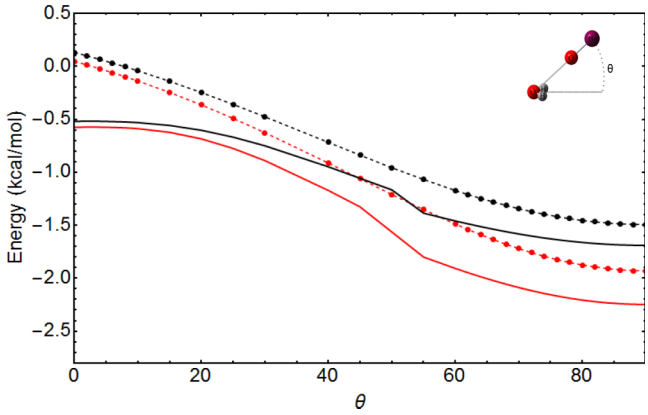

FIG. 7. Values of R_{OO}, θ, ϕ, θ', and ϕ' parameters taken from Table I - Scan 6. Red lines denote ground state and black curve denotes the excited state. Dashed curves are from RCCSD(T)/aug-cc-pVQZ with dots at the exact location of each data point, while solid curves are for mTTM potential energies.

Thus, as discussed in Sec. III C covering the test scan, this configuration is not a true local minimum but a saddle point at the intersection of this symmetric angle with the radial component, which can be seen in Scan 3.

It is worth mentioning that the global minimum has been reproduced well within the two PES: Scan 2 and Scan 5. Furthermore, the ground state minimum of both Scan 1 and Scan 3 are in good agreement with the optimized local minimum structure. The minima associated with the ground state of both Scan 3 and Scan 6 is the maximum of the test scan; this fact reinforces that the PES was capable of and did successfully capture the saddle point structure.

B. The description of the analytical potentials

Parameters for both the ground and the first excited states obtained from the fitting procedure for the $BrO{\cdot}H_2O$ complex in the mTTM potential are reported in Table II. Here, while modifying the potential, the parametrizations for the water molecule were kept unchanged, conforming to those of the TTM2-R function and only the parameters for the interaction between the BrO and the water molecules were calculated.

The first PES scan calculated by using mTTM potential is in good agreement with the RCCSD(T) curve. The fitted ground state BE at the minimum is −2.83 kcal/mol in deviation of −0.26 kcal/mol from RCCSD(T) energy; the excited state shows a deviation of +0.13 kcal/mol. The minimum occurs at 3.0 Å for the ground state and at 3.125 Å for the excited state, the ground state is shifted by −0.05 Å while the excited state agrees with the RCCSD(T) value. The maximum difference between the *ab initio* and the fitted energy values occurs at very large energies within the hard-shell regime of the potential for both the ground and excited states. Within the negative short-range, bonding and long range areas of the potential the largest deviation between fitted and *ab initio* energies occur at the minimum, this is consistent with previous works.

TABLE II. Parameters of the mTTM function fitted to described both the ground and excited states of the $BrO{\cdot}H_2O$ complex.

Parameter	Ground state	Excited state
M-O distance (Å)	0.504	0.879
Q_O (10^{-20} C)	−4.887	−5.894
Q_{Br} (10^{-20} C)	4.887	5.894
α^O_{XX} (Å^3)	0.074	0.567
α^O_{YY} (Å^3)	0.835	0.067
α^O_{ZZ} (Å^3)	0.075	0.565
α^{Br}_{XX} (Å^3)	2.986	0.207
α^{Br}_{YY} (Å^3)	3.185	0.207
α^{Br}_{ZZ} (Å^3)	2.251	3.063
σ_{OO} (Å)	2.816	2.884
ϵ_{OO} (kcal/mol)	0.565	0.676
σ_{OBr} (Å)	2.318	2.432
ϵ_{OBr} (kcal/mol)	2.630	1.557
n_1	11.078	14.195
m_1	3.834	4.574
σ_{HO} (Å)	1.725	1.682
ϵ_{HO} (kcal/mol)	0.354	0.162
n_2	11.723	10.985
m_2	5.282	6.105
σ_{HBr} (Å)	3.489	3.763
ϵ_{HBr} (kcal/mol)	0.063	0.045
n_3	9.604	11.128
m_3	7.313	6.723

In Scan 2, minimum occurs at 4.5 Å for the ground state with BE 4.52 kcal/mol with deviation of −0.06 Å in distance and −0.15 kcal/mol in energy from the *ab initio* values. For the excited state the deviation in $R_{O..O}$ and the energy is +0.1 Å and −0.001 kcal/mol, respectively. For Scan 3, the fitted ground state BE is 2.13 kcal/mol at a minimum of $R_{O..O}$ = 3.00 Å, with a deviation of −0.16 kcal/mol in BE and at the minimum of the *ab initio* calculations. The excited state energy is 0.13 kcal/mol lower than RCCSD(T) energy and the $R_{O..O}$ value at minimum is in deviation of 0.01 Å from the *ab initio* value. In the angular Scan 4, the ground state fitted curve shows minima at rough values of $\phi' = 80°$ and $\phi' = -68°$, additionally there exists a maximum at $\phi' = 0°$, in agreement with the RCCSD(T) curve. The ground state BEs of the minima are 3.27 kcal/mol and 2.69 kcal/mol which are in deviation of 0.02 kcal/mol and −0.15 kcal/mol from the RCCSD(T) energies for the minima at $\phi' = 80$ and $\phi' = -70$, respectively. The excited state of Scan 4 is characterized by a slow slope approach to a minimum value, the deviation in the minimum is 0.03 kcal/mol. The angular Scan 5 shows satisfactory agreement with the *ab initio* results. The ground state and excited state fitted curves show minimum at $\theta' = 94°$, a 1° deviation from the RCCSD(T) minimum value. The BEs of ground and excited states are deviate by −0.11 kcal/mol and +0.02 kcal/mol from the *ab initio* energies, respectively. Finally in Scan 6, both the ground state and excited state fit curves show minimum at $\theta = 90°$ similar to the RCCSD(T) curve. The ground state energy at the minimum shows a deviation of −0.31 kcal/mol while the excited state minimum energy shows a deviation of −0.20 kcal/mol with respect to the corresponding *ab initio* energies, while the entirety of the fitted curve is stationed below the *ab initio*.

Figure 8 displays the schematic depiction of errors, where the energy difference between the *ab initio* energy and our parameterized analytical potential is plotted against the *ab initio* energy all scans; the excited state errors are found above the ground state, and the assignments made within the legend apply globally. For the quantitative estimation of the error in mTTM potential, we calculated the average difference ($\overline{\Delta E}$), the average of the absolute difference ($\overline{|\Delta E|}$), the variance of the signed difference ($\Delta(\Delta E)$), and the maximum difference ($\max|\Delta E|$) between the analytical potential energies and RCCSD(T) energies. The values for both ground and excited state are reported in Table III. The *ab initio* energy is used as a cutoff (E_{cut}), for selecting a point data set. The maximum average error is −0.27 kcal/mol in ground state and −0.14 kcal/mol in the excite state. The maximum average unsigned error in ground state is 0.32 kcal/mol while it increased to 0.36 in the excited state. The small variances are consistent with the fact that the fitted potential smoothly and are overall acceptably tight. The absolute maximum error in the ground state (*viz.* 2.53 kcal/mol) comes from high in the

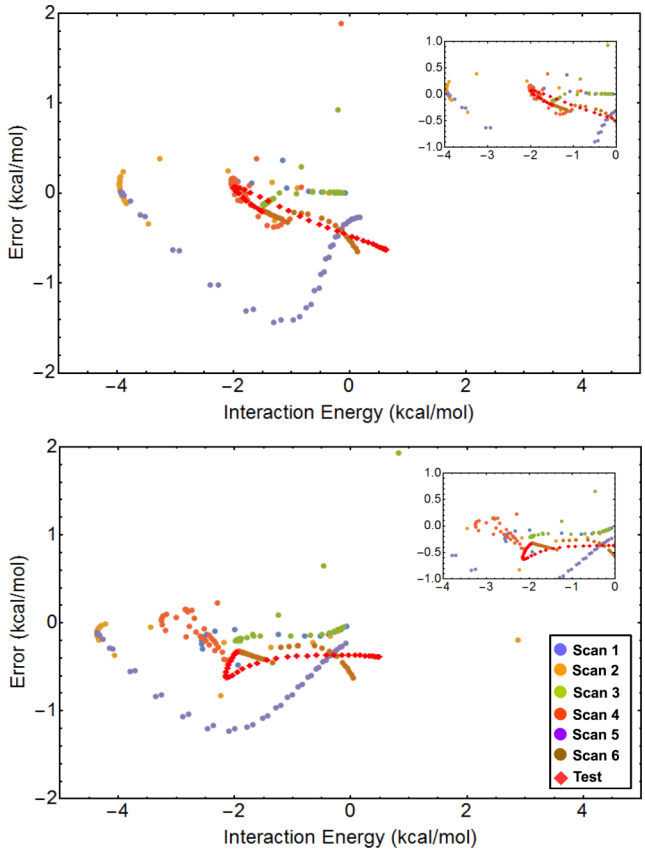

FIG. 8. Errors in the fitted ground (lower) and excited (upper) state potential energies as a function of the RCCSD(T) energy for each configuration in the PES training scans shown in Figures 2–7, as well as the test scan discussed in Sec. III C. The top plot is the schematic error for the excited state, while the bottom is for the ground state. Colors associated with the individual scans are noted in the legend and apply to both plots.

hard shell regime of Scan 2 and maximum error the excited (*viz.* 4.94 kcal/mol) is from the Scan 2 hard shell regime, as well. As even the *ab initio* values corresponding to these large error points are very high in energy, it is unlikely that these large deviations will ever be explored in a dynamic simulation. The low average errors indicate a high degree of reliability for the analytical potential, since all the energies of minima in all scans have been reproduced well. The lowest error in the minima of all scans is, +0.02 and −0.03 kcal/mol (from the ground states of Scan 5 and Scan 4, respectively) and highest error is −0.31 kcal/mol (from Scan 6's ground state). This quantitative analysis shows that the accuracy of mTTM potential developed for the $BrO{\cdot}H_2O$ complex falls between the accuracy of the previously characterized $OH{\cdot}H_2O$ and the $ClO{\cdot}H_2O$ potentials.[11,12] That the present errors fall within the values of the previously studied systems is suggestive of possible scaling in the error, i.e., this potential function may have difficulties in describing systems with larger charges.

In addition to the whole curve error analysis above, a Kolmogorov-Smirnov (KS) analysis[55] was performed to compare the *ab initio* data and the fitted mTTM curves for each scan and for each state. This requires that each potential energy curve be treated as a probability density function. N data points are sampled through each of the distributions. The Kolmogorov-Smirnov analysis allows one to determine if sampled points from two distributions are indeed sampled from the same distribution. This analysis requires that the sampled data be placed into a cumulative distribution function (CDF) prior to performing the Kolmogorov-Smirnov statistic on the two CDF's being compared, where the KS statistic is given by

$$d_{n,n} = \sup_{X \in N} |F_{1,n}(X) - F_{2,n}(X)|. \tag{8}$$

Within the above, $F_{1,n}(X)$ and $F_{2,n}(X)$ denote the two sample sets coming from the two distributions to be examined over the single variable X, indexed as 1 and 2 with n and n' sample points each. Effectively, $d_{n,n}$ is the maximum absolute deviation between the CDF's of the respective sample sets. The CDF's for each of the training sets in the ground state are given in Figure 9, where the black curves are the CDF's for the *ab initio* data and the red are the CDF's from the mTTM fittings. The distributions were sampled with $N = 1000$ and the CDF's were constructed with a bin number of 100. Figure 10 shows the same, but for the excited state scans. The values of d_{1000} for each of the training curves, as well as the location of the deviation, are given in Table IV; also within Table IV, is the information for the test curve, this to be discussed in Sec. III C. According to the Glivenko-Cantelli Theorem, if the sample sets are taken from the same distribution, then almost surely $d_{n,n} \to 0$ as $n \to \infty$. $d_{n,n}$ is then compared to specific values, $\alpha(N)$'s, generated at specific confidence intervals to determine

TABLE III. Average error ($\overline{\Delta E}$), mean unsigned error ($\overline{|\Delta E|}$), variance in average error distribution ($\Delta(\Delta E)$), and maximum absolute error ($Max(|\Delta E|)$) in the mTTM fit to the ground- and excited-state potentials as compared to the RCCSD(T)/aug-cc-pVQZ energies for all points N(E_{cut}) with either the mTTM or RCCSD(T)/aug-cc-pVQZ energy lower than the cutoff energy E_{cut}.

	Ground state					Excited state				
E_{cut}	$\overline{\Delta E}$	$\overline{\lvert\Delta E\rvert}$	$\Delta(\Delta E)$	Max($\lvert\Delta E\rvert$)	$N(E_{cute})$	$\overline{\Delta E}$	$\overline{\lvert\Delta E\rvert}$	$\Delta(\Delta E)$	Max($\lvert\Delta E\rvert$)	$N(E_{cute})$
−3	−0.16	0.17	0.0011	0.83	40	−0.004	0.13	0.0011	0.63	30
−2	−0.21	0.24	0.0011	1.23	88	−0.003	0.17	0.0014	1.02	53
−1	−0.27	0.29	0.0007	1.23	144	−0.09	0.22	0.0011	2.23	127
0	−0.26	0.30	0.0005	1.23	189	−0.14	0.27	0.0011	2.23	180
1	−0.26	0.30	0.0006	1.93	192	−0.14	0.29	0.0011	2.25	191
2	−0.25	0.30	0.0006	1.93	192	−0.14	0.29	0.0011	2.25	191
5	−0.25	0.32	0.0008	2.53	194	−0.07	0.36	0.0029	4.94	194

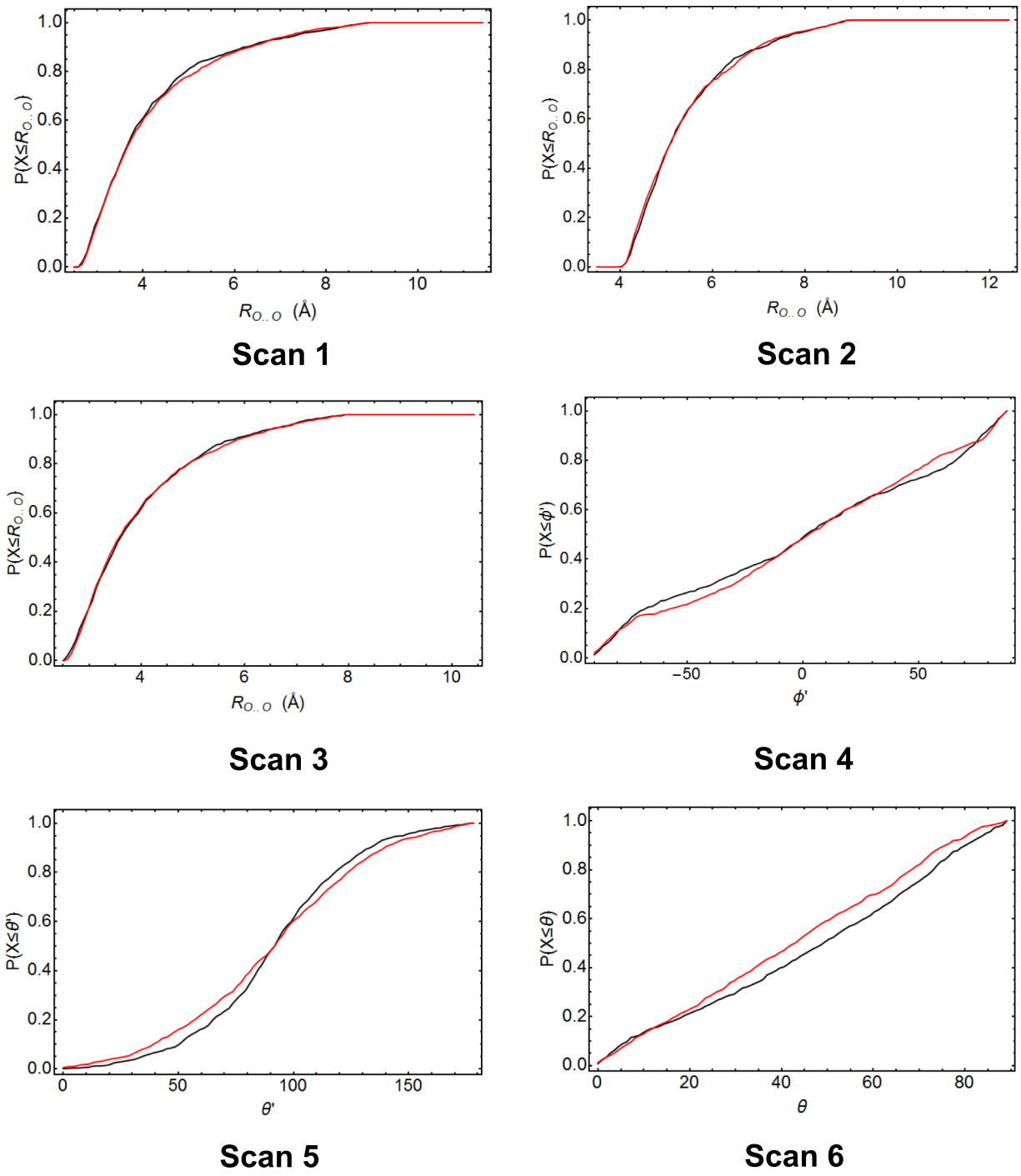

FIG. 9. CDF's used in the Kolmogorov-Smirnov analysis for the 6 scans employed to train the ground state mTTM fitting. The black curves are the CDF's related to the *ab initio* distribution, and the red curves are the CDF's related to the fitted mTTM distribution. Values for the maximum deviation, d_{1000}, and location of this maximum deviation are given in Table IV.

if the distributions are the same; we have tabulated several relevant values of $\alpha(N)$ within Table V for a continuous probability distribution.[56] As our mTTM fittings clearly do not share an identity relationship with the *ab initio* data, the expectation that all our fittings should satisfy this criteria is unjustifiable. Yet, the similarities in the CDF's, as well as the relatively low values in the $d_{n,n}$, speak to reasonably good agreement between the parent distributions. Scans 1-4, for both ground and excited states, display values sufficient to claim these distributions are the same, save the ground state of Scan 4. All remaining scans do not have a sufficiently small $d_{n,n}$ to support the claim of identical distributions, but are small enough to suggest that the fittings and *ab initio* data are highly correlated and similar; thus, the fittings are in agreement with the *ab initio* data.

C. Brief analysis of test scan for fitted potential

We have selected an angular scan with a reasonably difficult topology of the BE as a test case for our fitted

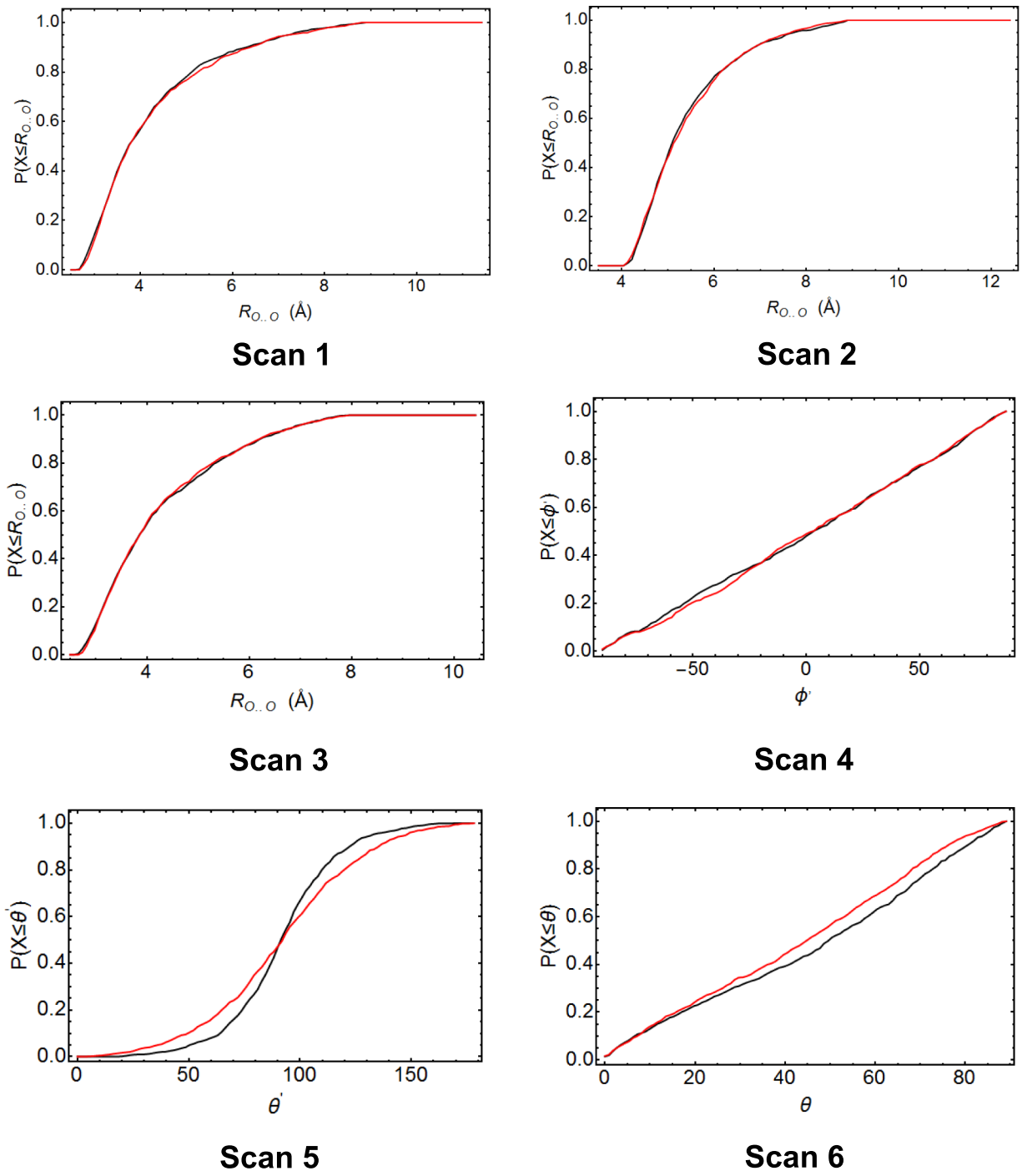

FIG. 10. CDF's used in the Kolmogorov-Smirnov analysis for the 6 scans employed to train the excited state mTTM fitting. The black curves are the CDF's related to the *ab initio* distribution, and the red curves are the CDF's related to the fitted mTTM distribution. Values for the maximum deviation, d_{1000}, and location of this maximum deviation are given in Table IV.

potential. The geometric variables for the test scan can be seen within Table I. In the angular test scan, the parameter ϕ is varied while maintaining the collinearity of Br–O_2–O_1 by setting ϕ equal to ϕ', essentially pin wheeling the OBr molecule around O_1 of water. The distance $R_{O..O}$ is set at 3.125 Å while both θ and θ' are set to 90° (see Figure 11). The two minima of the ground state are at 0° (2.11 kcal/mol) and at 270° (2.13 kcal/mol), while the minima of the excited state are located at 0° (1.98 kcal/mol) and at 260° (1.97 kcal/mol). The minima of the scan is clearly due to the stabilizing O_2–H interactions, while the maximum is due to the O_1–O_2 interactions, reaching their apex at $\phi = 128°$, near a C_{2v} symmetry point. The BEs of the minima in both states are slightly larger than those in the $ClO{\cdot}H_2O$ system, however, the energy splitting is similar. The maximum near 308° is found to have a similar configuration to the minimum of Scan 3; this, in turn, suggests that the minimum of Scan 3 is local minimum.

Within the fitted potential for the test scan, the ground state analytical potential curve show two minimum at $\phi = 0°$

TABLE IV. Presentation of the maximum deviations associated with a Kolmogorov-Smirnov analysis comparing the *ab initio* distribution to the mTTM distribution for all 7 scans discussed and for both states. Additionally, the location of the maximum deviation within distribution.

	Ground state		Excited state	
Scan number	d_{1000}	Location	d_{1000}	Location
1	0.034	5.20 Å	0.024	5.47 Å
2	0.029	6.47 Å	0.025	5.21 Å
3	0.021	2.82 Å	0.019	5.00 Å
4	0.059	−50.4°	0.036	−41.4°
5	0.065	111.6°	0.094	64.8°
6	0.085	48.6°	0.071	56.7°
Test scan	0.112	206.5°	0.055	−227.5°

TABLE V. Description of the statistical significance parameters for N = 1000. The first row is the level of statistical significance desired, the second row is the general form of the significance criteria, $\alpha(N)$, and the final row gives the numerical value associated with the desired level of significance.

Statistical significance parameters for N = 1000, 100 bins				
Significance intervals:	0.10	0.05	0.02	0.01
$\alpha(N)$	$\frac{1.22}{\sqrt{N}}$	$\frac{1.36}{\sqrt{N}}$	$\frac{1.51}{\sqrt{N}}$	$\frac{1.63}{\sqrt{N}}$
α_{1000}	0.038 58	0.043 01	0.047 75	0.051 55

and 260° in resembling the *ab initio* curve. The BEs at these minima deviate 0.61 and 0.59 kcal/mol from the RCCSD(T) energies at 0° and 260°, respectively. The excited state curve also shows the minima at $\phi = 0°$ and 260° identical to RCCSD(T) with a deviation in BEs of 0.07 and 0.06 kcal/mol, respectively; note that these low deviates are not characteristic of the curves, their overall topology displays a similar global deviation similar to the ground state curve. It is important to note that these curves overestimate the interaction energy but do so in a smooth and highly consistent manner and they replicate the general topology of this interaction scan well.

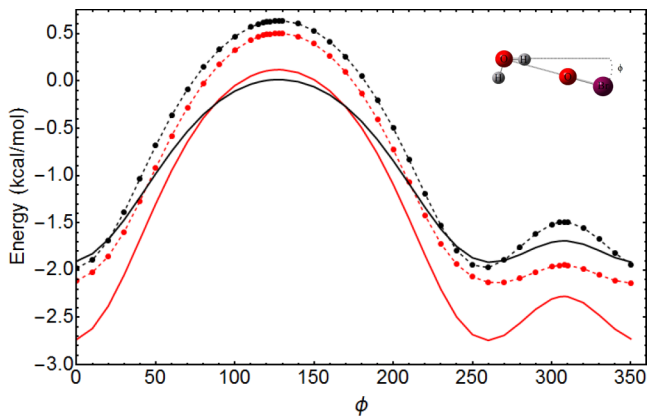

FIG. 11. Values of R_{OO}, θ, ϕ, θ', and ϕ' parameters taken from Table I test scan. Red lines denote ground state and black curve denotes the excited state. Dashed curves are from RCCSD(T)/aug-cc-pVQZ with dots at the exact location of each data point, while solid curves are for mTTM potential energies.

The nearly global shift in the interaction energy downward will not effect this variable scan within a search for optimal configuration, as the topology remains consistent, as do the rough values for the angular binding energies from the maximum of the scan. As can be seen in Figure 8, the errors associated with the test scan's mTTM fitting are within the bounds of the errors for the training scans. The CDFs associated with ground and excited state comparisons between the *ab initio* and mTTM fittings are shown in Figure 12; the values of the deviations and their locations are given in Table IV. These values are not satisfactory to support the hypothesis that the underline distributions are identical, but they do support the assertion from the error analysis that these distributions are both related and correlated. Additionally, the excited state fit is better than the ground state.

D. Comparison of ground state BrO parameters with OH and ClO

Here we shall briefly compare the parameters associated with the ground state BrO-complex potential with those from the OH and ClO potentials.[11,12] As can be seen from the Table VI, atomic charges are slightly higher in BrO than ClO, yet lower than OH, clearly following the electronegativity trend. The charge on the oxygen atom is -5.92×10^{-20} C in OH while it is -3.216×10^{-20} C in ClO and -4.887×10^{-20} C for the BrO radical. The M-O distance in BrO radical is largest, and is smallest for the OH radical. This suggests that the "M" site is shifting towards the halogen atom, in order of atomic size. The relationship between the "M" site location and the size of the atom in question is likely to be in response to a number of factors, including: an extending bond length, the on-set of the hard shell regime of the potential and increasing polarizabilities along the bond axis in the ground state. The non-exponential terms within the Lennard-Jones potential are consistent with chemical intuition for the systems. The oxygen-oxygen Lennard-Jones interaction is highly constrained to a region conforming to fixed exponential values, as this is a known acceptable range for this interaction. The O–H interaction is roughly well characterized in previous works, yet does vary with reference to the charge of the oxygen atom, as the charges in the water molecule are consistent between the works. The ϵ_{OH} is slightly larger than those of the other systems, while the crossing value is fairly consistent implying a similar onset to attraction, but a lower minimum to the potential. The bromine-oxygen interaction potential in the description of the system, ϵ_{OBr}, is a large interaction with an accordingly large value, of 2.24 kcal/mol; the crossing value, considering the ϵ, is suggestive of an attractive interaction during the typical proximities of these atoms with the scans performed. Additionally, ϵ_{BrH} is very low, while its crossing value is fairly high with reference to typical distances within the scans; this being consistent with sampling this Lennard-Jones term for repulsive values. All values for the excited state fittings are appreciably diminished or increased with trends consistent to those observed in the OCl radical system, and verified using the higher-valued excited state *ab initio* energies as reference.

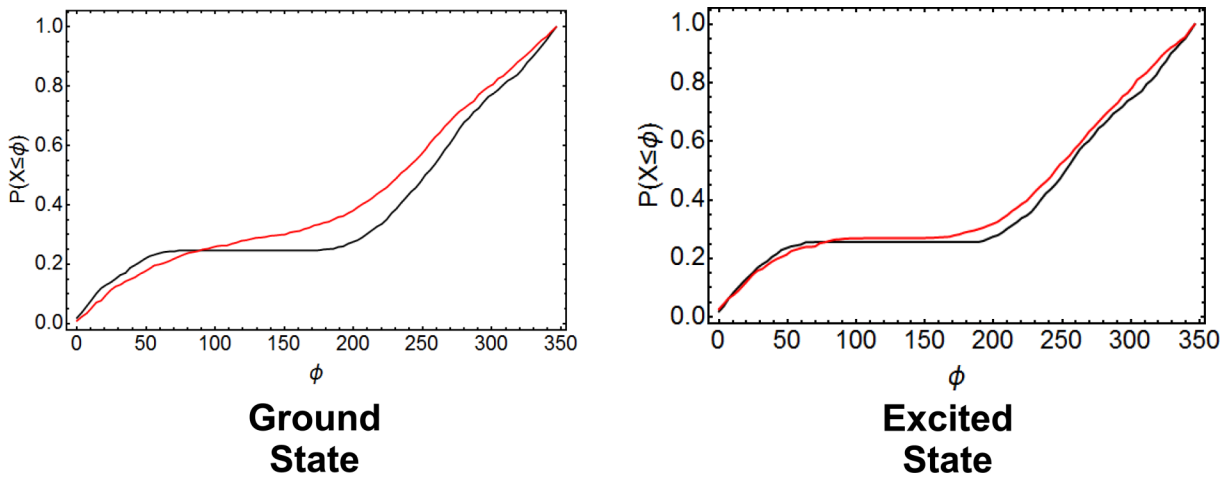

FIG. 12. CDF's used in the Kolmogorov-Smirnov analysis for the test scan. The black curves are the CDF's related to the *ab initio* distribution, and the red curves are the CDF's related to the fitted mTTM distribution. Values for the maximum deviation, d_{1000}, and location of this maximum deviation are given in Table IV.

TABLE VI. Comparison of ground state parameters from the mTTM fitted functions for the BrO·H_2O, ClO·H_2O and OH·H_2O systems.

Parameter	BrO	ClO	OH
M-O distance (Å)	0.504	0.407	0.132
Q_O (10^{-20} C)	−4.887	−3.216	−5.92
Q_{Br} (10^{-20} C)	4.887	3.216	5.92
α^O_{XX} (Å^3)	0.074	0.074	0.074
α^O_{YY} (Å^3)	0.835	1.477	2.223
α^O_{ZZ} (Å^3)	0.075	0.074	0.148
α^{Br}_{XX} (Å^3)	2.986	4.446	0.074
α^{Br}_{YY} (Å^3)	3.185	2.848	0.296
α^{Br}_{ZZ} (Å^3)	2.251	0.148	0.074
σ_{OO} (Å)	2.816	2.986	2.912
ϵ_{OO} (kcal/mol)	0.565	0.186	0.575
σ_{OBr} (Å)	2.318	2.567	1.852
ϵ_{OBr} (kcal/mol)	2.630	0.961	0.126
n_1	11.078	10.35	9.0
m_1	3.834	4.0	4.0
σ_{HO} (Å)	1.725	2.001	1.799
ϵ_{HO} (kcal/mol)	0.354	0.193	0.201
n_2	11.723	9.0	9.4
m_2	5.282	4.0	4.2
σ_{HBr} (Å)	3.489	3.295	...
ϵ_{HBr} (kcal/mol)	0.063	0.050	...
n_3	9.604	9.01	...
m_3	7.313	5.61	...

IV. CONCLUSIONS

This work presents an analytic potential energy function for the interaction between a BrO radical and a water molecule. This interaction potential was generated by modifying the preexisting Thole-type model first used to describe water. The one-dimensional PES scans were generated for both the ground and the excited electronic states of the BrO·H_2O complex at the RCCSD(T)/aug-cc-pVQZ level of theory. The characteristics of the PES scans reveals many similarities between the BrO·H_2O system and the previously parameterized OH·H_2O and ClO·H_2O systems. The fitted analytical potential shows good agreement with the *ab initio* results. This analytic potential was developed to facilitate future simulations involving the interaction between BrO radical and water clusters; these simulations are presently underway in our group. This work should be useful in discerning and investigating possible novel chemistries taking place at the water interface of clouds within the atmosphere involving the bromine oxide radical.

ACKNOWLEDGMENTS

The authors are grateful to the National Science Foundation (Project No. CHE-1500217) for financial support. Computational support from the Hansen and the Carter clusters at Purdue University is gratefully acknowledged. The authors would also like to thank both our editor and our reviewers for providing a great deal of helpful criticism.

[1]L. A. Barrie, J. W. Bottenheim, R. C. Schnell, P. J. Crutzen, and R. A. Rasmussen, Nature **334**, 138 (1988).
[2]M. Hausmann and U. Platt, J. Geophys. Res. **99**, 25399, doi:10.1029/94JD01314 (1994).
[3]S. Solomon, Nature **347**, 347 (1990).
[4]U. Platt and C. Janssen, Faraday Discuss. **100**, 175 (1995).
[5]U. Platt and G. Hönninger, Chemosphere **52**, 325 (2003).
[6]W. Stumm and J. J. Morgan, Aquatic Chemistry: Chemical Equilibria and Rates in Natural Waters (John Wiley & Sons, Inc., New York, 1995), p.1040.
[7]M. J. Molina and F. S. Rowland, Nature **249**, 810 (1974).
[8]S. P. Sander, R. R. Friedl, and Y. L. Yung, Science **245**, 1095 (1989).
[9]R. Escribano, R. G. Mosteo, and P. C. Gómez, Can. J. Phys. **79**, 597 (2001).
[10]R. Kopitzky, H. Grothe, and H. Willner, Chem. - Eur. J. **8**, 5601 (2002).
[11]S. Du, J. S. Francisco, G. K. Schenter, T. D. Iordanov, B. C. Garrett, M. Dupuis, and J. Li, J. Chem. Phys. **124**, 224318 (2006).
[12]S. Du, J. S. Francisco, G. K. Schenter, and B. C. Garrett, J. Chem. Phys. **126**, 114304 (2007).
[13]Y. Li and J. S. Francisco, J. Chem. Phys. **115**, 8381 (2001).
[14]J. S. Francisco and S. P. Sander, J. Am. Chem. Soc. **117**, 9917 (1995).
[15]L. Kaleschke, A. Richter, J. Burrows, O. Afe, G. Heygster, J. Notholt, A. M. Rankin, H. K. Roscoe, J. Hollwedel, T. Wagner, and H.-W. Jacobi, Geophys. Res. Lett. **31**, L16114, doi:10.1029/2004gl020655 (2004).
[16]R. J. Cicerone, Rev. Geophys. **19**, 123, doi:10.1029/RG019i001p00123 (1981).
[17]R. J. Salawitch, Nature **439**, 275 (2006).
[18]X. Yang, R. A. Cox, N. J. Warwick, J. A. Pyle, G. D. Carver, F. M. O'Connor, and N. H. Savage, J. Geophys. Res. **110**, D23311, doi:10.1029/2005jd006244 (2005).

[19]D. J. Lary, M. P. Chipperfield, R. Toumi, and T. Lenton, J. Geophys. Res. **101**, 1489, doi:10.1029/95JD02839 (1996).
[20]M. J. Prather and R. T. Watson, Nature **344**, 729 (1990).
[21]W. T. Sturges, D. E. Oram, L. J. Carpenter, and S. A. Penkett, Geophys. Res. Lett. **27**, 2081, doi:10.1029/2000GL011444 (2000).
[22]M. W. Chase, J. Phys. Chem. Ref. Data **25**, 1069 (1996).
[23]Y. Ohshima, K. Sato, Y. Sumiyoshi, and Y. Endo, J. Am. Chem. Soc. **127**, 1108 (2005).
[24]C. S. Brauer, G. Sedo, E. M. Grumstrup, K. R. Leopold, M. D. Marshall, and H. O. Leung, Chem. Phys. Lett. **401**, 420 (2005).
[25]M. D. Marshall and M. I. Lester, J. Phys. Chem. B **109**, 8400 (2005).
[26]D. P. Schofield and H. G. Kjaergaard, J. Chem. Phys. **120**, 6930 (2004).
[27]P. D. Cooper, H. G. Kjaergaard, V. S. Langford, A. J. McKinley, T. I. Quickenden, and D. P. Schofield, J. Am. Chem. Soc. **125**, 6048 (2003).
[28]H. Fu, Z. Zhou, and X. Zhou, Chem. Phys. Lett. **382**, 466 (2003).
[29]S. Du, J. S. Francisco, G. K. Schenter, and B. C. Garrett, J. Am. Chem. Soc. **131**, 14778 (2009).
[30]M. H. Matus, M. T. Nguyen, D. A. Dixon, K. A. Peterson, and J. S. Francisco, J. Phys. Chem. A **112**, 9623 (2008).
[31]J. R. McKeachie, M. F. Appel, U. Kirchner, R. N. Schindler, and T. Benter, J. Phys. Chem. B **108**, 16786 (2004).
[32]S. Aloisio and J. S. Francisco, Acc. Chem. Res. **33**, 825 (2000).
[33]O. Gálvez, A. Zoermer, and H. Grothe, J. Phys. Chem. A **110**, 8818 (2006).
[34]O. Gálvez, P. C. Gómez, and L. F. Pacios, J. Comput. Chem. **30**, 2538 (2009).
[35]C. Hampel and H.-J. Werner, J. Chem. Phys. **104**, 6286 (1996).
[36]K. Raghavachari, G. W. Trucks, J. A. Pople, and M. Head-Gordon, Chem. Phys. Lett. **157**, 479 (1989).
[37]G. E. Scuseria, Chem. Phys. Lett. **176**, 27 (1991).
[38]P. J. Knowles, C. Hampel, and H.-J. Werner, J. Chem. Phys. **99**, 5219 (1993).
[39]C. J. Burnham, J. Li, S. S. Xantheas, and M. Leslie, J. Chem. Phys. **110**, 4566 (1999).
[40]C. J. Burnham and S. S. Xantheas, J. Chem. Phys. **116**, 1479 (2002).
[41]S. S. Xantheas, C. J. Burnham, and R. J. Harrison, J. Chem. Phys. **116**, 1493 (2002).
[42]C. J. Burnham and S. S. Xantheas, J. Chem. Phys. **116**, 1500 (2002).
[43]R. A. Kendall, T. H. Dunning, and R. J. Harrison, J. Chem. Phys. **96**, 6796 (1992).
[44]D. E. Woon and T. H. Dunning, J. Chem. Phys. **98**, 1358 (1993).
[45]M. Schütz and H.-J. Werner, Chem. Phys. Lett. **318**, 370 (2000).
[46]M. Schütz and H.-J. Werner, J. Chem. Phys. **114**, 661 (2001).
[47]G. Hetzer, M. Schütz, H. Stoll, and H.-J. Werner, J. Chem. Phys. **113**, 9443 (2000).
[48]J. da Silva Gomes, R. Gargano, J. B. L. Martins, and L. G. M. de Macedo, J. Phys. Chem. A **118**, 5818 (2014).
[49]B. A. Hess, P. Chandra, and R. J. Buenker, Mol. Phys. **52**, 1177 (1984).
[50]J. P. Desclaux and N. Bessis, Phys. Rev. A **2**, 1623 (1970).
[51]M. Pernpointner, J. Phys. B: At., Mol. Opt. Phys. **38**, 1955 (2005).
[52]T. Fleig, D. Edvardsson, S. T. Banks, and J. H. Eland, Chem. Phys. **343**, 270 (2008), theoretical Spectroscopy and its Impact on Experiment (in honour of Sigrid D. Peyerimhoff).
[53]H.-J. Werner, P. J. Knowles, G. Knizia, F. R. Manby, and M. Schtz, Wiley Interdiscip. Rev.: Comput. Mol. Sci. **2**, 242 (2011).
[54]H.-J. Werner, P. J. Knowles, G. Knizia, F. R. Manby, M. Schütz *et al.*, MOLPRO, version 2012.1, a package of *ab initio* programs, 2012, see http://www.molpro.net.
[55]D. Zwillinger and S. Kokoska, *CRC Standard Probability and Statistics Tables and Formulae* (Champman & Hall/CRC, New York, USA, 1999).
[56]P. D. T. O'Connor and A. Kleyner, *Practical Reliability Engineering* (John Wiley & Sons, Ltd., West Sussex, United Kingdom, 2011), pp. 455–456.